Effect of thermal environments on fast charging Li-ion batteries

Teng Liu,[1] Shanhai Ge,[1] Xiao-Guang Yang,[1,3] and Chao-Yang Wang[1,2,4] *

[1]Electrochemical Engine Center (ECEC) and Department of Mechanical Engineering, The Pennsylvania State University, University Park, PA 16802

[2]EC Power, 341 Science Park Road, State College, PA 16803, USA

[3]Present address: National Engineering Laboratory for Electric Vehicles, School of Mechanical Engineering, Beijing Institute of Technology, Beijing 100081, China

*Corresponding author. Tel.: +1 814 863 4762; Fax: +1 814 863 4848. Email: cxw31@psu.edu

Highlights

- Evaluate the cooling requirement and temperature uniformity of fast charging LiBs.
- Predict the fast-charging capability of LiBs under different thermal environments.
- Propose a thermal modulation method to achieve fast charging with zero cooling.

Abstract

Battery thermal management systems (BTMSs) are expected to keep the battery temperature at a moderate level (~30°C) to minimize the thermally exacerbated degradation. However, during fast charging, a strong cooling system is required to restrict the temperature rise of Li-ion batteries (LiBs), which significantly increases the cost and weight of battery packs, and induces a large temperature variation inside the battery. In this work we find that all these drawbacks could be relieved by allowing LiBs to charge at higher temperatures. Since the fast charging of a LiB only takes a tiny fraction of its lifetime, the aging rate is limited even at a charging temperature of 60°C. Three types of thermal environments are proposed: kept constant at 30°C, preheated to 60°C, and adiabatic fast charging. With

an experimentally validated electrochemical-thermal (ECT) coupled model, we explore the interplay between thermal management and the fast-charging performance. It is found that a gradually increasing temperature profile is the best option to balance the lithium plating and thermal management of the battery. Combining adiabatic fast charging with a preheating step, we can achieve minimal cooling need, perfect temperature uniformity within a battery, and fast-charging capability simultaneously.

Keywords: Li-ion battery; fast charging; thermal management; lithium plating; numerical modeling

1 Introduction

With a continuous improvement of energy density, Li-ion batteries (LiBs) have become ubiquitous in our life. Apart from all kinds of electronic devices, LiBs are powering up millions of electric vehicles (EVs) on the road [1] and even electrify urban air transport in the future [2,3]. However, the long charging time is still a critical factor that constrains the user experience, hindering broader adoption of LiBs [4]. The next-generation LiBs should attain high energy density and fast-charging capability simultaneously [1].

One of the challenges for fast charging is how to deal with the massive heat generation that comes from high charging currents [5]. Since the heat originating from ohmic loss is proportional to the square of the current, reducing the charging time by an order of magnitude would result in an increase in heat generation rate by a hundredfold. It is expected that the battery thermal management systems (BTMSs) for fast charging LiBs should possess much higher cooling capacities than the existing systems so as to keep the battery in an optimum temperature range around 30°C [6]. Researchers have proposed to use liquid cooling or phase change materials (PCMs) to enhance the cooling and limit the temperature rise during fast charging [7–9]. However, compared with air cooling, liquid cooling and PCMs significantly increase the cost and weight of BTMSs. Besides, the temperature nonuniformity is proportional to the heat flux along the thermal boundary; in other words, strong cooling could enlarge spatial variation of temperature within LiBs, causing nonuniform aging rates within the battery pack.

In a recent study, we discovered that by elevating the cell temperature to ~60°C during fast charging, the required heat transfer coefficient and heat flux of cooling could be reduced by 12 and 3 times, respectively [10]. Although LiBs degrades faster at elevated temperatures due to the accelerated growth of the solid-electrolyte interface (SEI) layer, the SEI growth is a function of time, which could be limited owing to extremely short operation time of fast charging [11]. Some exothermal reactions, such as decomposition of SEI layers, could be triggered at 90°C or above, causing irreversible damage to the cell within a single cycle [12]. While around 60°C, the LiBs could survive more than 1,000 hours of cycling

[10,13,14], which could translate into thousands of cycles with fast charging at 60°C [3,10]. Specifically, for a battery constantly cycled at 60°C, it experiences 2 hours of accelerated aging for each cycle, and will reach its end of life after e.g. 500 cycles due to SEI growth; whereas for a battery with 10-minute fast charging at 60°C and discharged at room temperature, the time of accelerated SEI growth for each cycle is 10 minutes as well, and the corresponding cycle life can reach 6,000. This theory has been validated experimentally; with heated fast charging, the cell has only 8.3% capacity loss after 2,500 cycles [10]. In other words, it may not be necessary to constrain the maximum battery temperature rise as long as it is still well below 90°C and the exposure time to the high temperature is short. Thus, it appears that battery cooling during fast charging warrants scrutiny.

In this work, we consider three kinds of thermal environments for fast charging. The first one has no cooling components, and all the thermal boundaries are assumed to be adiabatic to approximate the minimum cooling condition. The second one has a very strong cooling system, which starts working once the battery temperature reaches 30°C and maintains the surface temperature at 30°C thereafter. The third one has an internal heater; the battery is rapidly preheated to 60°C prior to fast charging and subsequently maintained at the elevated temperature by an appropriate cooling condition during fast charging. We shall use an experimentally validated electrochemical-thermal (ECT) coupled model to examine the three thermal environments and predict their temperature evolution, cooling need, and temperature variation of LiBs, respectively. It is worth noting that the presence of lithium plating, a hazardous side reaction when the charge rate exceeds the maximum capability of lithium insertion [15–17], is strongly influenced by the thermal condition of the battery [18,19]; thus, we will also include the onset charge rate of lithium plating in our analysis. The goal is to find out the most optimized BTMS design for fast charging LiBs.

2 Model development and experimental validation

The ECT model used in this work describes the 1D electrochemical processes through the porous electrode, with Li diffusion in spherical particles accounted for by the so-called pseudo-2D approach [20,21]. The governing equations have been widely introduced in our previous work [22–24]. Here we

give a brief introduction to the numerical model for brevity (the description for each term in the governing equations can be found in the "List of Symbols").

- The reaction current (i) is related to the surface overpotential by the Butler-Volmer equation. Where the exchange current density (i_0) determines the kinetics of lithium insertion/deintercalation at the active material/electrolyte interface.

$$i = i_0 \left[\exp\left(\frac{\alpha_a F}{RT} \eta \right) - \exp\left(-\frac{\alpha_c F}{RT} \eta \right) \right] \quad (1)$$

- The surface overpotential (η) is the potential difference between the solid and electrolyte phase at the reaction interface, driving electrochemical reaction. When $\eta > 0$, the reaction is dominated by the anodic reaction (lithium deintercalation); when $\eta < 0$, the reaction is dominated by the cathodic reaction (lithium insertion).

$$\eta = \Phi_s - \Phi_e - U - iR_f \quad (2)$$

- Effective parameters in a porous medium are expressed as a function of porosity and Bruggeman exponents to account for tortuosity. Higher porosity results in higher effective transport values in the electrolyte but smaller effective values in the solid phase.

$$\Psi_s^{eff} = (1-\varepsilon)^p \Psi_s, \Psi_e^{eff} = \varepsilon^p \Psi_e \quad (3)$$

- Volumetric current density (j) is the source term in charge conservation equations, which can be obtained by multiplying the specific surface area (a_s) with the electrode current density. The value of a_s is computed by assuming spherical particles.

$$j = a_s i,\ a_s = 3(1-\varepsilon)/r_i \quad (4)$$

- Charge conservation in the solid phase describes the voltage drop caused by the ohmic resistance in electrodes. Usually, the potential drop in the solid phase is much smaller than that in the electrolyte phase, and thus is negligible.

$$\frac{dI_s}{dx} = \frac{d}{dx}\left(-\sigma^{eff}\frac{d\Phi_s}{dx}\right) = -j \tag{5}$$

- Charge conservation in the electrolyte consists of two parts: the first part describes the voltage drop caused by the ohmic resistance in the electrolyte; the second part describes the concentration overpotential, which comes from the concentration gradient of the electrolyte.

$$\frac{dI_e}{dx} = \frac{d}{dx}\left(-\kappa^{eff}\frac{d\Phi_e}{dx} - \kappa_D^{eff}\frac{d\ln c_e}{dx}\right) = j,$$
$$\text{where } \kappa_D^{eff} = \frac{2RT\kappa^{eff}}{F}\left(t_+^0 - 1\right)\left(1 + \frac{d\ln f_{\pm}}{d\ln c_e}\right) \tag{6}$$

- Species conservation in the electrolyte is governed by a diffusion process, with a non-zero migration term if the transference number (t_+) for Li-ion is less than one. The distribution of electrolyte concentration (c_e) is described by this equation, which determines the magnitude of concentration overpotential. The surface kinetics is also influenced by the value of c_e.

$$\frac{d}{dt}\left(\varepsilon c_e\right) = \frac{d}{dx}\left(D_e^{eff}\frac{dc_e}{dx}\right) + \left(\frac{1-t_+^0}{F}\right)j \tag{7}$$

- Species conservation in the active material particles is given by Fick's law. The value of lithium stoichiometry in solid particles is determined by this equation. The equilibrium potential of the active material is determined by the lithium stoichiometry on the particle surface.

$$\frac{\partial c_s}{\partial t} = \frac{1}{r^2}\frac{\partial}{\partial r}\left(r^2 D_s\frac{\partial c_s}{\partial r}\right), -D_s\frac{\partial c_s}{\partial r}\bigg|_{r=R_0} = \frac{i}{F} \tag{8}$$

- Heat generation is calculated by the equation below. The heat generation comes from four components, namely: heat generation at the reaction interface, ohmic heat generation through the solid electrodes, heat generation through the electrolyte, and reversible heat.

$$\dot{Q}_{gen} = A_E \int_0^L \left(\dot{\phi}_i + \dot{\phi}_s + \dot{\phi}_e + \dot{\phi}_{rev} \right) dx$$
$$\dot{\phi}_i = j(\Phi_s - \Phi_e - U)$$
$$\dot{\phi}_s = I_s(-\frac{d\Phi_s}{dx}) = \sigma_s^{eff}(\frac{d\Phi_s}{dx})^2 \quad (9)$$
$$\dot{\phi}_e = I_e(-\frac{d\Phi_e}{dx}) = \kappa^{eff}(\frac{d\Phi_e}{dx})^2 + \kappa_D^{eff}\frac{d\ln c_e}{dx}\frac{d\Phi_e}{dx}$$
$$\dot{\phi}_{rev} = j(T\frac{dU}{dT})$$

- The energy conservation equation determines the evolution of battery temperature in the form of a lumped model.

$$mc_p \frac{dT}{dt} = \dot{Q}_{gen} - h(T - T_\infty) A_s \quad (10)$$

- The thermal dependence of electrochemical properties is described by the Arrhenius equation. With the battery temperature solved by the lumped thermal model, the electrochemical properties are updated according to:

$$\Psi(T) = \Psi_{ref} \exp\left(\frac{E_{act}}{R}(\frac{1}{T_{ref}} - \frac{1}{T}) \right) \quad (11)$$

- The onset of lithium plating is determined by the lithium deposition potential. When $\eta_{Li|Li+} < 0$ V (or the surface overpotential of lithium insertion exceeds the equilibrium potential on graphite surface), Li-ions start to deposit on the graphite surface [3].

$$\eta_{Li|Li+} = U - |\eta_{LixC6|Li+}| \quad (12)$$

The ECT model described above is solved with GT-Autolion, a commercial simulation package [25]. Using the design parameters of an energy-dense LiB (271 Wh/kg if scaled to 50-Ah format) [26], we set up a model and validate it with the experimental results of rate performance tests. These results were measured using 4-Ah experimental cells. We built the smaller test cells consisting of the same electrodes and electrolyte for saving of materials and convenience of experimentation, However, all results can be

extrapolated to the 50-Ah design which is similar to actual cells used in EV applications [27]. The fully charged cell is discharged under various discharge rates and measurement techniques fully described in our previous work [23]. As shown in Fig. 1, the simulation results adequately predict the voltage and temperature profiles under various discharge rates. The design and modeling parameters of the battery are listed in Table 1, 2 and Fig. S1, S2. [19,28–36].

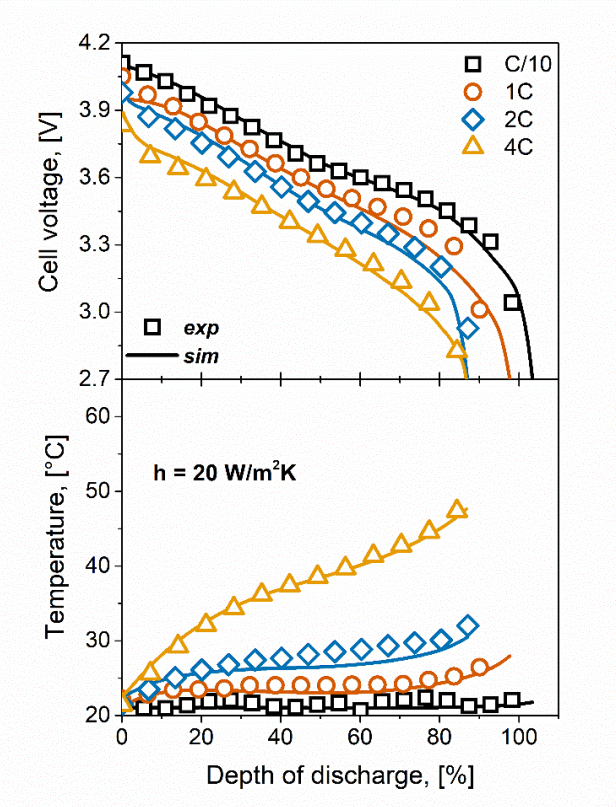

Fig. 1 – Validated ECT model with voltage and temperature profiles of rate performance tests. Experimental data attained from discharging the battery at room temperature under various rates.

Table 1 - Design parameters for the energy-dense LiB

Parameters	Anode	Separator	Cathode
Composition	artificial graphite (Gr)	Celgard-2325	$LiNi_{0.8}Mn_{0.1}Co_{0.1}O_2$ (NMC811)
Weight fraction of the active materials	97.7 wt%	-	97.7 wt%
Specific capacity, [mAh/g]	350	-	203
Porosity, ε	0.26	0.40	0.30
Areal loading capacity, [mAh/cm^2]	3.75	-	3.4
Electrolyte composition	1M LiPF6 in EC/EMC (3:7 by wt.) + 2wt% VC		
Specific energy of cell (4-Ah test cell), [Wh/kg]	237		
Specific energy of cell (50-Ah cell), [Wh/kg]	271		

Properties	Graphite (Li_xC_6)	Separator	$Li_xNi_{0.8}Mn_{0.1}Co_{0.1}O_2$
Particle radius, r [μm]	10 A	-	3 B
Exchange current density, i_0 [mA/cm^2]	$0.21[2x^{0.5}c_e^{0.5}(1-x)^{0.5}]$ C [19,28]	-	$0.2[2x^{0.5}c_e^{0.5}(1-x)^{0.5}]$ B
Activation energy of i_0, $E_{act}^{i_0}$ [kJ/mol]	65 C [29,30]	-	65 B
Charge transfer coefficient, α_a, α_c	0.5, 0.5 A	-	0.5, 0.5 A
Solid state diffusivity, D_s [cm^2/s]	$2e\text{-}10\ (1.5\text{-}x)^{1.5}$ C [31]	-	$2e\text{-}10\ (1.5\text{-}x)^{1.5}$ B
Activation energy of D_s, $E_{act}^{D_s}$ [kJ/mol]	38 C [32]	-	21 B
Film resistance, R_f [Ωcm^2]	0 A	-	0 A
Bruggeman factor, p	2.2 C [33]	2 C [33]	2.1 B
Specific heat of cell, c_p [J/(kg·K)]	1200 C [36]		
A, measured/calculated/commonly-used values. B, fitted from simulation-experiment comparison. C, obtained from the literature.			

Table 2 -Modeling parameters for active materials and separator

3 Results and Discussion

3.1 Fast charging LiBs under different thermal environments

Battery performance varies significantly under different thermal environments, especially when it comes to fast charging. The internal resistance of LiBs is closely related to the battery temperature. Due to the large charging current, changes in internal resistance could cause notable impacts on voltage profile, heat generation rate, and lithium deposition potential.

Fig. 2(a) depicts three temperature profiles corresponding to the three different cooling strategies during 3C charging. The ambient temperature and the initial temperature of the battery both remain constant at 20°C. In the first case with no cooling, heat generated during charging is converted into the internal energy of the battery, causing the maximum temperature rise to around 50°C when the battery reaches the cut-off voltage. The temperature profile for the second case consists of two sections. In the beginning, we assume there is no cooling, and the temperature profile coincides with the first case. Active cooling is then activated when the battery temperature reaches 30°C and is sufficiently large to maintain a constant temperature. For the third case, the battery is preheated prior to charging and then kept at 60°C during charging.

The voltage profiles under the different thermal environments are plotted in Fig. 2(b). The voltage loss decreases with elevation of battery temperature and enables the battery to take in more energy before reaching the cut-off voltage limit. If the battery is kept at 30°C, the battery can only reach 50% state of charge (SOC) when it hits the cut-off voltage, while the final SOCs under the adiabatic condition and preheating to 60°C are 80% and 90%, respectively.

In addition to less energy get charged, large voltage loss also results in higher heat generation rates. The cooling should balance the heat generation to maintain a steady battery temperature. The

requisite heat dissipation rates under different conditions, as plotted in Fig. 2(c), are averaged at 0.132 and 0.035 W/cm^3, respectively, for keeping at 30°C and preheating to 60°C cases. Thus, the cooling need is much reduced either by increasing the operating temperature or allowing temperature elevation during charging.

Fig. 2(d) shows the evolution of lithium deposition potential. According to Eq. (12), lithium plating is prone to happen with small equilibrium potential or large surface overpotential on graphite. Higher charging temperatures could significantly lower the surface overpotential. Consequently, for battery charging at 60°C, the lithium deposition potential is always above the onset line, while for the battery charging at 30°C, lithium plating exists during the majority of the charging process. For the battery with an adiabatic boundary condition, lithium plating happens in the beginning of charging when the battery temperature is still low.

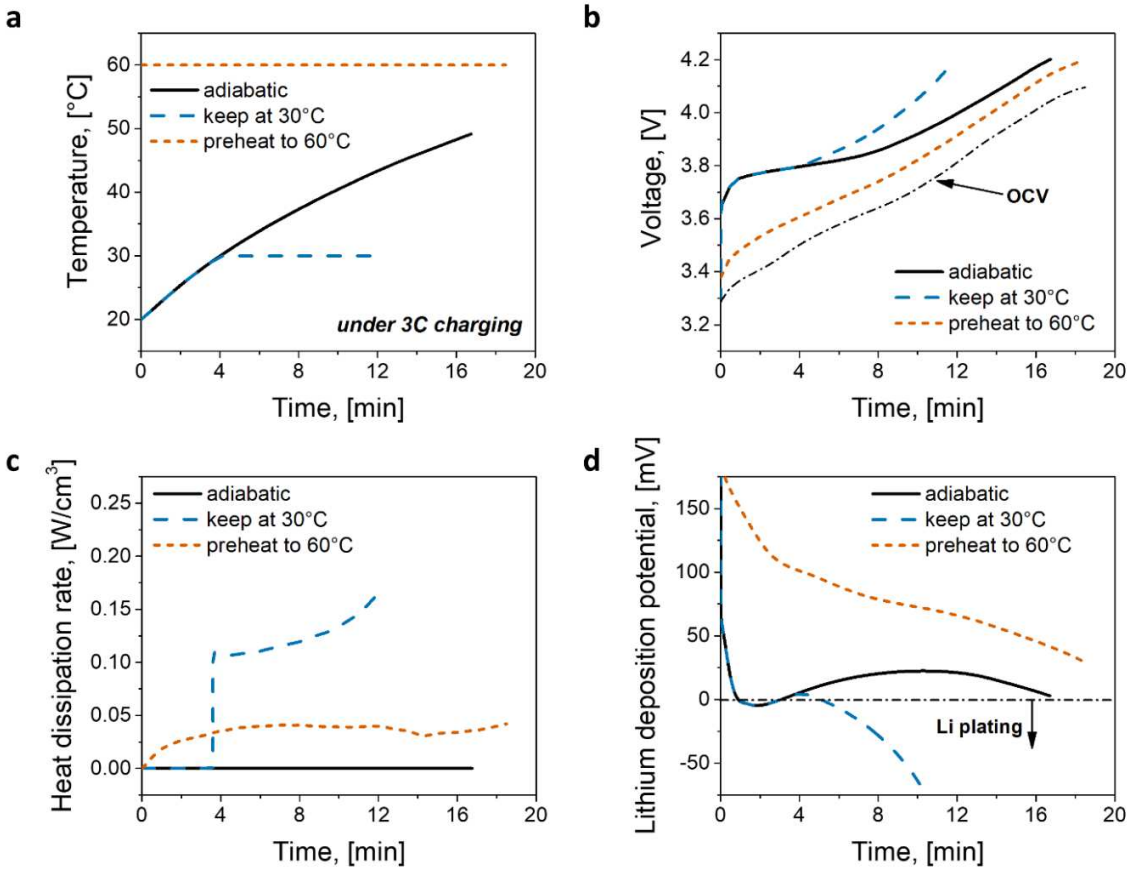

Fig. 2 – Battery behaviors under 3C fast charging with different thermal environments. (a) temperature profiles. (b) voltage profiles. (c) requisite volumetric heat dissipation rates. (d) evolution of lithium deposition potentials.

The pros and cons for fast charging the batteries under different thermal environments can be summarized as follows. When keeping the battery temperature at 30°C, the degradation owing to SEI layer growth is negligible; however, the requirement for cooling is high, and the battery has severe degradation mainly due to lithium plating. In contrast, if we elevate the charging temperature to 60°C, the degradation is dominated by SEI growth, but it is beneficial to lower the cooling requirement and avoid battery degradation due to lithium plating. For the battery under the adiabatic condition, the advantage is that the battery needs no cooling, and there is no spatial temperature variation within the battery; the aging rates caused by lithium plating and SEI growth both lie between the former two cases.

3.2 Temperature uniformity and heat transfer requirements during fast charging

Temperature uniformity and the required heat transfer coefficient are two crucial factors in designing BTMSs for fast charging LiBs. In the ECT model, we used a lumped analysis for the battery (Eq. (10)) to predict the heat generation and temperature evolutions under various charging conditions. In this subsection, we introduce a 1D heat transfer model to estimate spatial temperature variation inside a battery cell. Specifically, we assume that the cooling is applied only from in-plane or through-plane direction from the outer surface of the battery. With the prescribed thermal profiles on battery surface (Dirichlet boundary condition), the required heat transfer coefficients for cooling and the corresponding center temperatures can be calculated as functions of cell dimensions.

Under the adiabatic condition, the batteries have perfect temperature uniformity with no need for thermal management. While if we want to keep the battery temperature constant, the generated heat must be fully removed from the battery; we can calculate the corresponding heat transfer coefficient and temperature distribution within the battery if the characteristic length for heat conduction is given. As shown in Fig. S3, the characteristic length, L_C, equals to half of the cell thickness if the heat flux is applied in the through-plane direction, and equals to half of the cell width if the heat flux is applied in the in-plane direction. The governing equation for 1D heat transfer is given below.

$$\frac{dT}{dt} = \alpha \frac{dT}{dx^2} + \frac{\dot{q}_{gen}}{\rho c_p}, \text{ where } \alpha = \frac{k}{\rho c_p} \tag{13}$$

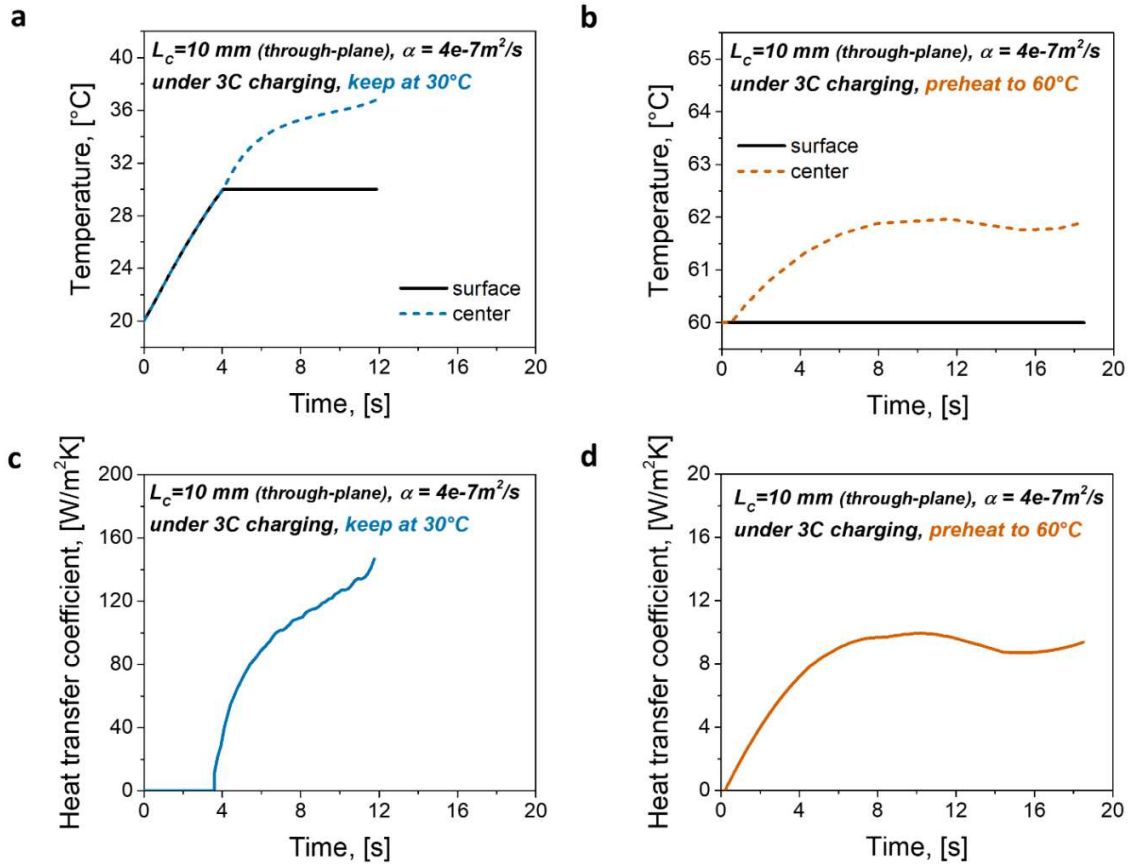

Fig. 3 – Temperature uniformity and cooling requirements for a 20-mm cell under 3C charging. (a, b) temperature variations between surface and cell center when keeping the surface temperature at 30°C and 60°C. (c, d) required heat transfer coefficients when keeping the surface temperature at 30°C and 60°C

Assume a battery under 3C charging is cooled along the through-plane direction; the cell thickness is 20 mm (L_C = 10 mm). The maximum temperature variation within the battery occurs between half-thickness of the cell and the cooling surface. Suppose the thermocouple is mounted on the battery surface for feedback control. In that case, we can calculate the variation of battery temperature under different thermal environments as plotted in Fig. 3(a), 3(b). When keeping the battery temperature at 30°C, the maximum spatial variation is ~7°C, which drops to ~2°C if we elevate the charging temperature to 60°C. The required heat transfer coefficients for cooling are given in Fig. 3(c) and 3(d). For battery

charging at 30°C, the maximum heat transfer coefficient reaches 150 W/m^{2}K, which can be achieved only with strong forced convection of air or liquid cooling. When charging at 60°C, the required heat transfer coefficient drops to ~10 W/m^{2}K (a 15-fold reduction), which could be easily achieved with air natural convection.

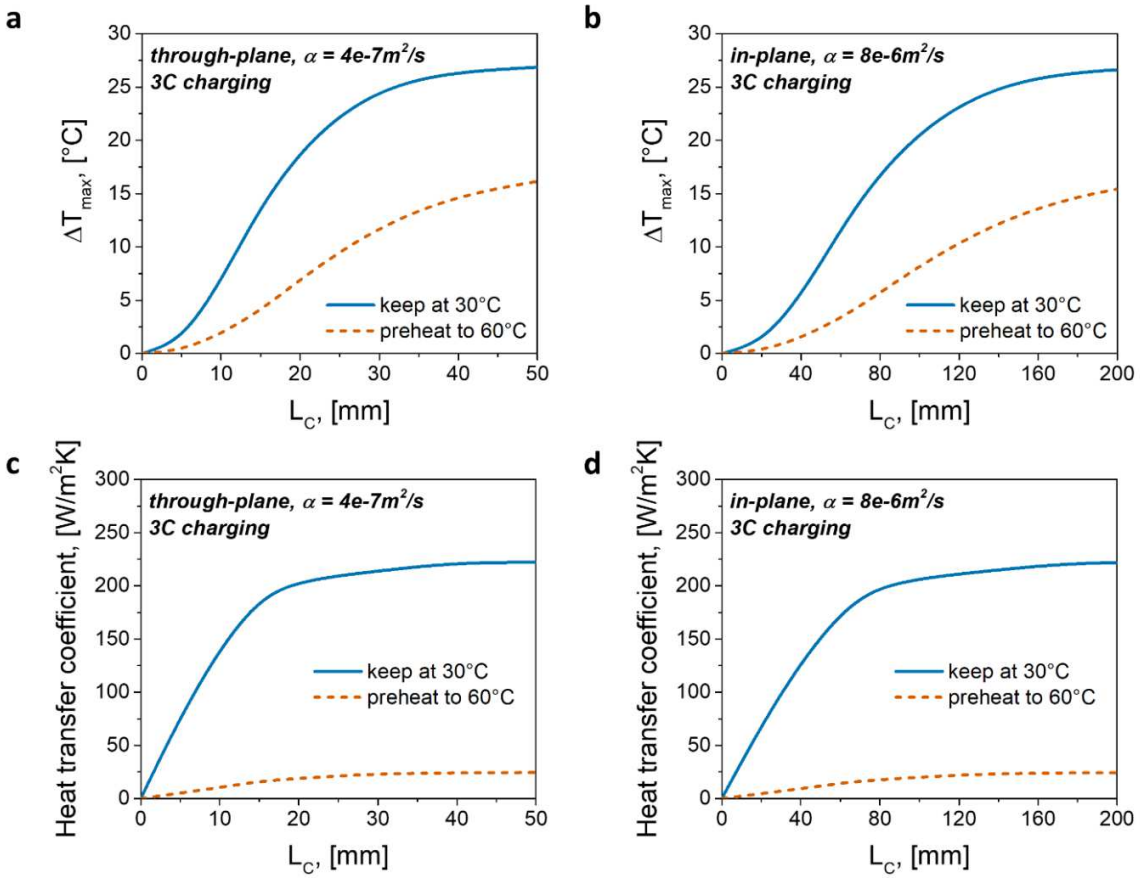

Fig. 4 – Thermal behavior under different cell dimensions. (a, b) Maximum temperature variations within the battery vs. characteristic length in through-plane and in-plane directions. (c, d) Required heat transfer coefficients for cooling vs. characteristic length in through-plane and in-plane directions.

To describe the thermal behavior of batteries with larger thickness under fast charging, we plot the maximum temperature variations and the required heat transfer coefficients vs. L_C, as shown in Fig. 4. The characteristic time for thermal diffusion is given by $\tau = (L_C)^2/\alpha$; the thermal behavior in different

directions would be identical if the characteristic time is the same. The thermal diffusivity through the in-plane direction is about 20 times larger than the through-plane direction. So, if the width of the cell is larger than 4.5 times ($20^{0.5}$ ~ 4.5) of the cell thickness, the cooling should be applied in the through-plane direction, and vice versa. For practical battery cells with the thickness ranging from 10 to 30 mm, this implies that the present assumption of dominant through-plane heat transfer is valid for cell width greater than 45 and 135 mm, respectively. There is a rapid growth of temperature variation and cooling need as the characteristic lengths getting larger. Although larger cell formats are beneficial to increase the energy density of batteries, if the battery is required to keep at a constant temperature, the characteristic length in the cooling direction should be kept small to have a uniform temperature distribution and low cooling needs.

3.3 Fast charging capability under different thermal environments

In this subsection, we are going to evaluate the fast-charging performance of LiBs by calculating the battery SOC, at which lithium plating first occurs, vs. the charge rate. For a given thermal environment, the cell is simulated under a consecutive set of charge rates. For each case, the lithium plating potential (LDP) predicted with Eq. (12) is a function of the final SOC. When LDP drops to zero, the corresponding SOC is plotted as that at the onset of Li plating in Fig.5 as dashed lines. Fig. 5 also depicts the maximum SOC with constant-current charging as solid lines. Thus, the areas between solid lines and dashed lines indicate the SOC range of lithium plating under different charge rates. Such 2D diagrams reflect the fast-charging capabilities under various thermal environments.

If the batteries are charged from 0% SOC, the maximum charge rates without lithium plating under adiabatic, keeping at 30°C, and preheating to 60°C cases are predicted to be 2.9C, 1.8C, and 4.1C respectively (Fig. 5). It is noteworthy that batteries under the adiabatic condition could achieve a reasonable charge rate without any cooling or heating components and maintain a uniform temperature at the same time; therefore, can we just charge the batteries without any thermal management?

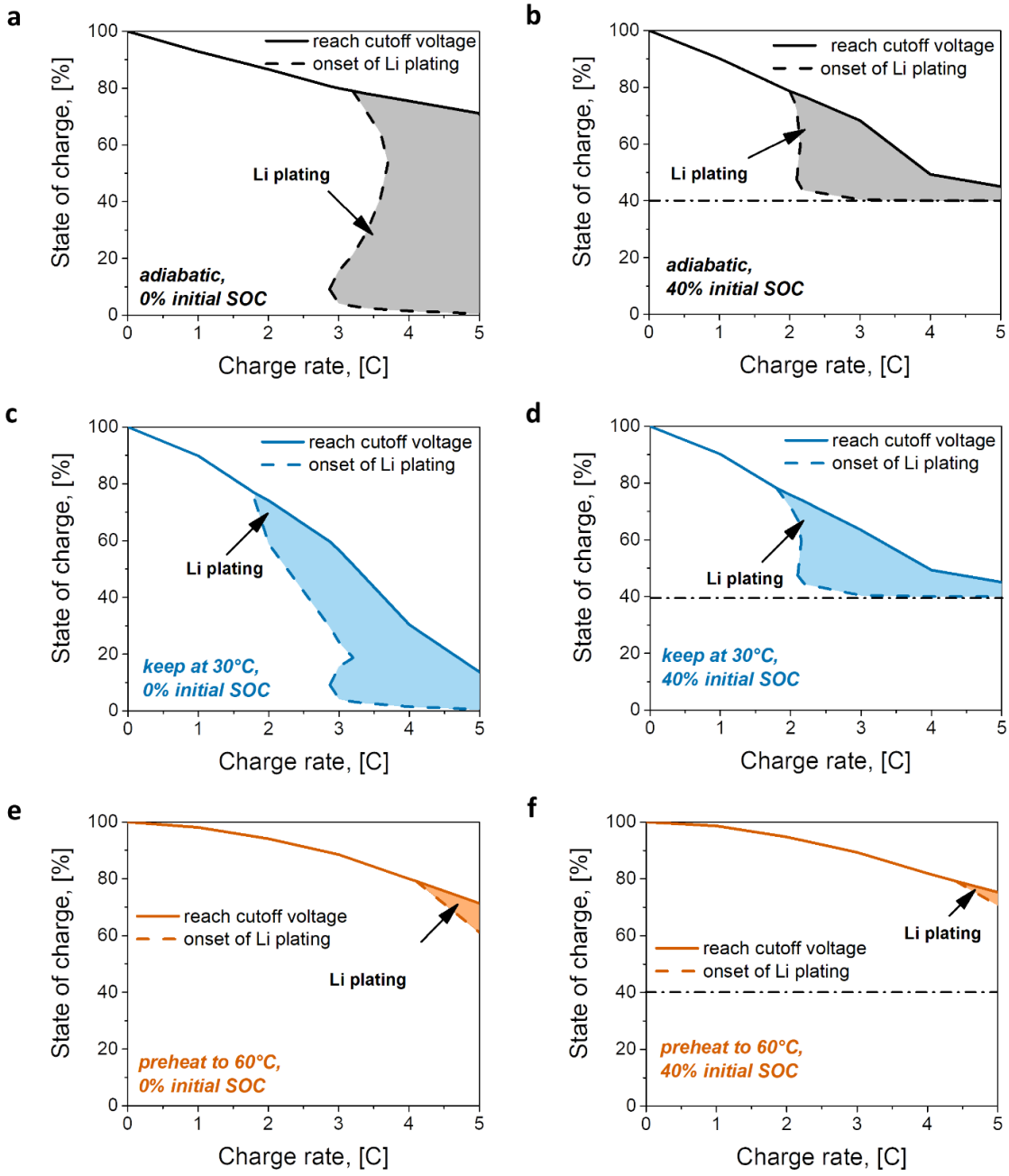

Fig. 5 – Maps of fast charging capability. (a, b) Charging the battery from 0% and 40% SOC under the adiabatic condition. (c, d) Charging the battery from 0% and 40% SOC when keeping the battery at 30°C. (e, f) Charging the battery from 0% and 40% SOC after preheating the battery to 60°C

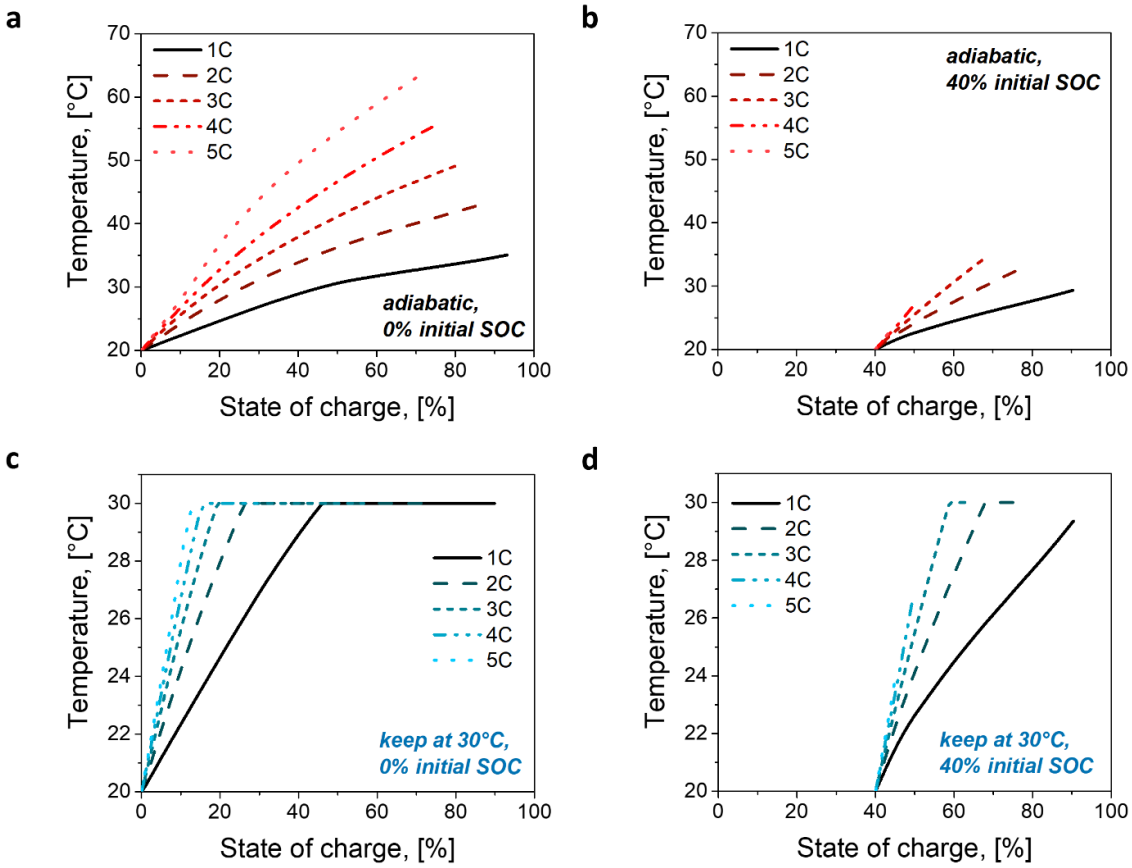

Fig. 6 – Temperature profiles when charging the battery at different C-rates. (a, b) Charging from 0% and 40% SOCs under the adiabatic condition. (c, d) Charging from 0% and 40% SOCs and keep the maximum temperature at 30°C.

A drawback of the battery in the adiabatic environment is that it would be very sensitive to the initial condition. As shown in Fig. 5(b), if we start charging the battery from 40% SOC rather than 0%, the maximum charge rate under the adiabatic condition drops from 2.9C to 2C. According to Eq. (12), lithium plating is more likely to occur at higher SOCs due to the decrease of equilibrium potential on the graphite surface. When the initial SOC equals to 40%, there is no time for the battery to heat up itself, and the battery temperature is not high enough to avoid lithium plating. As shown in Fig. 6, there is a remarkable drop of battery temperature during adiabatic charging after increasing the initial SOC from 0% to 40%. For instance, under 3C charging, the maximum temperature drops from 50°C to 35°C. If we

change the initial temperature of the battery to 0°C, the decay of fast charging capability is even more significant, with maximum charge rate drops below 1C (Fig. S4). In contrast, the preheated battery always has the same temperature profile during charging regardless of initial conditions; thus, we would expect a stable fast-charging performance under all circumstances.

3.4 Adiabatic fast charging with preheating

Allowing temperature rise during charging could reduce cooling needs and temperature variations, but the fast-charging capability varies with initial conditions. To solve this issue, it is instructive to preheat the battery to a moderate temperature before adiabatic fast charging, which requires zero cooling and permits fast charging under any initial conditions. The preheating temperature varies under different charge rates and initial conditions. As shown in Fig. 7(a) and 7(b), the temperature rise during adiabatic charging becomes larger with the increase of charge rate, and we can lower the preheating temperature to keep the maximum temperature at 60°C. While if the charge rate is fixed, the temperature rise becomes smaller at higher initial SOCs and we will increase the preheating temperature accordingly. The detailed temperature profiles are plotted in Fig. 7(c) and 7(d).

More generally, we can estimate the preheating temperature with Eq. (14), where T_{max} denotes the maximum temperature, T_0 denotes the initial temperature, ΔT_h denotes the temperature rise during preheating, and ΔT_{ad} denotes the temperature rise during adiabatic heating. When operating at low rates, the energy efficiency of the battery could exceed 99%, and the fraction of irreversible heat is less than 1% of the energy charged into the battery; while as we elevate the charge rate, the fraction of heat generation (H) increases rapidly and reaches ~9% at 5C charging (Fig. 7e), resulting in a larger temperature rise during adiabatic charging. Similarly, a wider SOC range (ΔSOC) or larger specific energy (SE) will also lead to a more significant change of battery temperature after fast charging.

$$T_{\max} = T_0 + \Delta T_h + \Delta T_{ad}, \Delta T_{ad} = \frac{\Delta SOC * SE * H}{c_p} \tag{14}$$

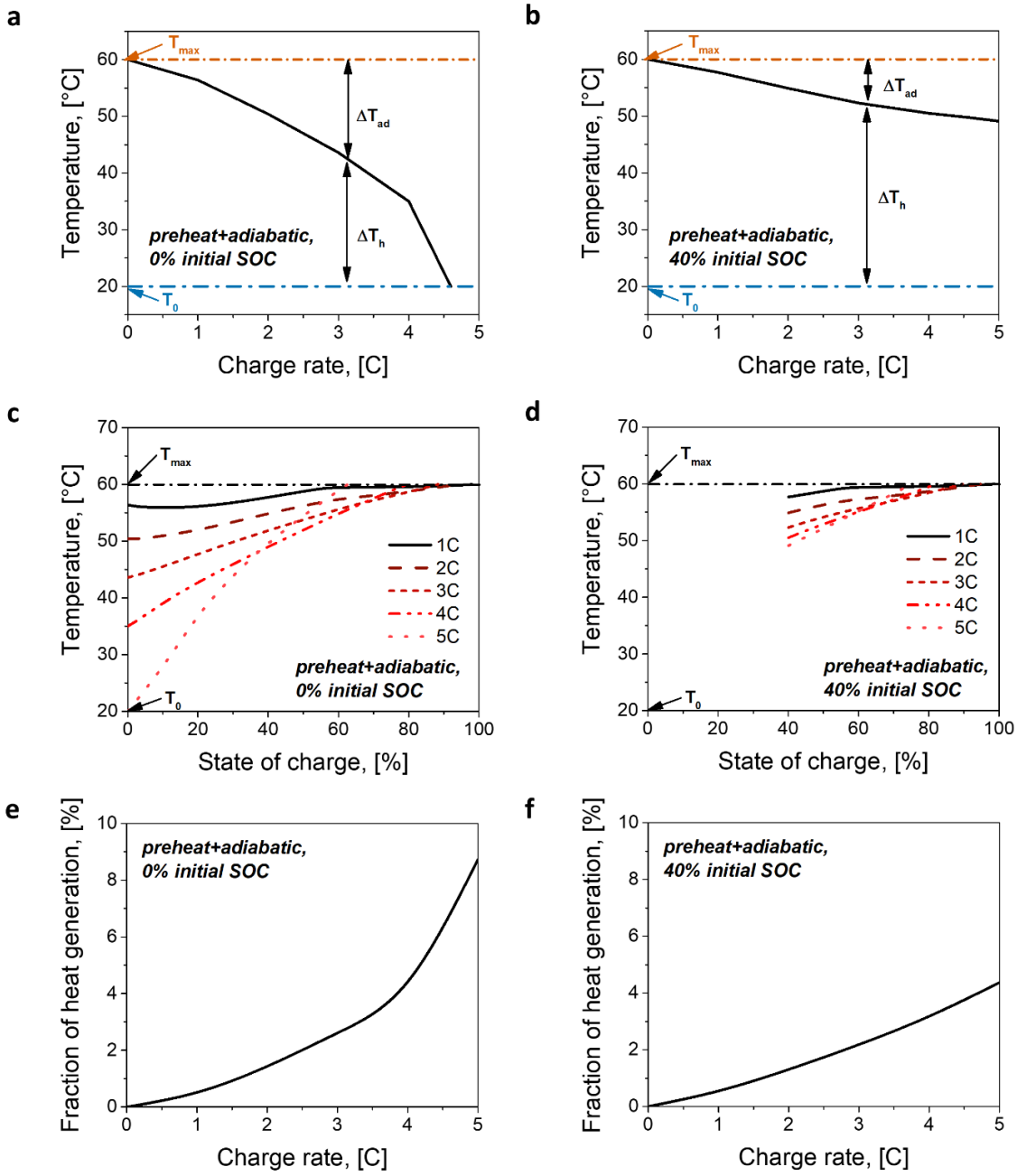

Fig. 7 – Adiabatic fast charging after preheating. (a, b) Preheating temperature when charging from 0% and 40% SOCs. (c, d) Temperature profiles with initial SOCs at 0% and 40%. (e, f) Fractions of heat generation during charging with initial SOCs at 0% and 40%.

Due to the high equilibrium potential on graphite surface at low SOCs, it could be unnecessary to heat up the cell to 60°C from the beginning. During adiabatic charging, the battery temperature gradually increases with SOC, offsetting the drop of equilibrium potential. The idea is similar to the multistage constant current (MCC) charging, where the charging currents decrease consecutively to accommodate the reduction of graphite potential, and get the maximum fast-charging capability at different SOC ranges [37]. The maps of fast charging capability under adiabatic charging with a preheating step are plotted in Fig. 8; the maximum charge rates without lithium plating with 0% and 40% SOCs are 3.9C and 4.3C, respectively, which is very close to the battery with a constant charge temperature at 60°C (4.1C charging from 0% SOC and 4.4C charging from 40% SOC). To sum up, adiabatic charging reduces the average battery temperature without sacrificing the rate capability. More importantly, with adiabatic charging, we can obtain minimal cooling and perfect temperature uniformity within the battery, which remarkably reduces the BMTS weight and enables us to make single cells in larger formats.

Granted, the preheating process consumes extra energy. According to Eq. (14), elevating the battery temperature by 10°C consumes 1.2% of the energy stored in the battery, which means the extra energy consumption is 4.8% if the temperature rise is 40°C during preheating. However, note that the energy for preheating comes from roadside chargers, so the preheating process will not affect the cruising range of EVs; rather, this gives consumers another choice to shorten their charging time by slightly increasing the amount of electricity they pay (~5%). Cooling after heated charge is by means of air natural convection or aspirated convection during driving, under a very large temperature difference, and hence consumes no battery energy.

The main challenge to realizing thermal modulation in fast charging is to heat up the cell quickly. A heating rate of 1°C/s could be achieved with an internal heating structure introduced in our previous study [38]. This method is also applicable for large format batteries; the temperature nonuniformity could be controlled within a reasonable level by embedding multiple heater sheets inside the battery [39].

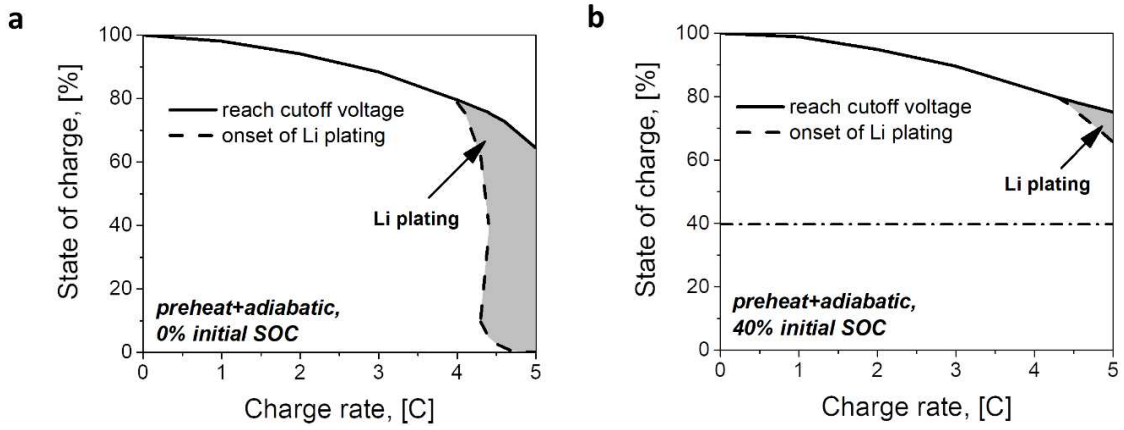

Fig. 8 – Maps of fast charging capability under adiabatic thermal conditions. (a) 0% initial SOC. (b) 40% initial SOC.

4 Conclusions

Thermal management for fast charging should not only pursue high cooling capacities but also consider the effect of thermal environments. Limiting the maximum temperature at 30°C brings little benefit, considering the large heat transfer coefficient required for the system and the low charge rate causing the onset of lithium plating. Using the battery performance at 30°C as a baseline, if we increase the battery temperature to 60°C, the temperature variation and cooling need will be reduced to 1/3 and 1/15 of the reference, while the maximum charge rate doubles. Although elevated temperatures accelerate the SEI layer growth, short charging time limits the exposure time of LiBs to high temperatures. As such, we expect very little impact on SEI-induced battery degradation over the lifetime.

By allowing the maximum temperature excursion to 60°C, there are multiple ways to modulate the battery temperature during fast charging. One is that we can allow the battery to heat up itself during charging, which greatly lowers the cooling needs and spatial temperature variations within the battery. Noting that lithium plating is more likely to happen at higher SOCs, the temperature profile of a LiB under the adiabatic environment benefits the fast-charging capability. With low initial temperatures or high initial SOCs, the fast-charging capability under adiabatic charging is considerably constrained. A

more robust strategy is to add a preheating step before adiabatic charging, which enables fast charging of LiB with zero cooling and perfect temperature uniformity regardless of initial conditions.

Acknowledgments

Financial support from the US Department of Energy's Office of Energy Efficiency and Renewable Energy (EERE) under award number DE-EE0008355 is gratefully acknowledged and the William E. Diefenderfer Endowment. We are also grateful to Gamma Technologies for offering GT-AutoLion™ software.

Author contributions

T. L. and C.-Y.W. conceived the idea and wrote the manuscript. T.L. and X.-G.Y. developed the validated model. S.G. fabricated the cells.

List of Symbols

Symbol	**Description**
A_E	total electrode area
a_s	specific surface area (SSA)
A_S	total surface area
c_e	electrolyte concentration
c_p	specific heat
c_s	ion concentration in solid phase
D_e	ionic diffusivity
D_s	solid diffusivity
E_{act}	activation energy
F	Faraday constant.
$f_{\pm}$	activity coefficient
h	convective heat transfer coefficient
H	fraction of heat generation
i	reaction current density.
i_0	exchange current density.
I_e	superficial current density in electrolyte
I_s	superficial current density in solid phase
L_c	characteristic length for heat conduction
p	Bruggeman exponent
$\dot{Q}_{gen}$	total heat generation rate
$\dot{q}_{gen}$	volumetric heat generation rate
R	universal gas constant.
R_f	film resistance.
r_i	particle radius
SE	specific energy
t_+	transference number of cations
U	equilibrium potential vs. $E^{\circ}_{Li\|Li+}$
α	thermal diffusivity
α_a, α_c	(anodic/cathodic) apparent transfer coefficients.
ε	porosity
η	surface overpotential.
$\eta_{Li\|Li+}$	lithium deposition potential
$\eta_{LixC6\|Li+}$	surface overpotential of lithium insertion on graphite
κ	ionic conductivity
κ_D	diffusional ionic conductivity
ρ	density
σ	electrical conductivity
Φ_s, Φ_e	solid phase/electrolyte potential
Ψ_s, Ψ_e	solid/electrolyte phase parameters

References

[1] J. Deng, C. Bae, T. Miller, Electric Vehicles Batteries : Requirements and Challenges, Joule. 4 (2020) 511–515. https://doi.org/10.1016/j.joule.2020.01.013.

[2] W.L. Fredericks, S. Sripad, G.C. Bower, V. Viswanathan, Performance Metrics Required of Next-Generation Batteries to Electrify Vertical Takeoff and Landing (VTOL) Aircraft, ACS Energy Lett. 3 (2018) 2989–2994. https://doi.org/10.1021/acsenergylett.8b02195.

[3] T. Liu, X. Yang, S. Ge, Y. Leng, C. Wang, Ultrafast charging of energy-dense lithium-ion batteries for urban air mobility, ETransportation. 7 (2021) 100103. https://doi.org/10.1016/j.etran.2021.100103.

[4] M. Li, M. Feng, D. Luo, Z. Chen, Perspective Fast Charging Li-Ion Batteries for a New Era of Electric Vehicles, Cell Reports Phys. Sci. 1 (2020) 100212. https://doi.org/10.1016/j.xcrp.2020.100212.

[5] M. Keyser, A. Pesaran, Q. Li, S. Santhanagopalan, K. Smith, E. Wood, S. Ahmed, I. Bloom, E. Dufek, M. Shirk, A. Meintz, C. Kreuzer, C. Michelbacher, A. Burnham, T. Stephens, J. Francfort, B. Carlson, J. Zhang, R. Vijayagopal, K. Hardy, F. Dias, M. Mohanpurkar, D. Scoffield, A.N. Jansen, T. Tanim, A. Markel, Enabling fast charging – Battery thermal considerations, J. Power Sources. 367 (2017) 228–236. https://doi.org/10.1016/j.jpowsour.2017.07.009.

[6] J. Warner, Thermal Management, in: Handb. Lithium-Ion Batter. Pack Des., Elsevier, 2015: pp. 115–130. https://doi.org/10.1016/B978-0-12-801456-1.00010-5.

[7] A. Tomaszewska, Z. Chu, X. Feng, S. O'Kane, X. Liu, J. Chen, C. Ji, E. Endler, R. Li, L. Liu, Y. Li, S. Zheng, S. Vetterlein, M. Gao, J. Du, M. Parkes, M. Ouyang, M. Marinescu, G. Offer, B. Wu, Lithium-ion battery fast charging: A review, ETransportation. 1 (2019) 100011. https://doi.org/10.1016/j.etran.2019.100011.

[8] S. Chen, N. Bao, A. Garg, X. Peng, L. Gao, A Fast Charging–Cooling Coupled Scheduling Method for a Liquid Cooling-Based Thermal Management System for Lithium-ion Batteries, Engineering. (2020). https://doi.org/10.1016/j.eng.2020.06.016.

[9] Y. Bao, Y. Fan, Y. Chu, C. Ling, X. Tan, S. Yang, Experimental and Numerical Study on Thermal and Energy Management of a Fast-Charging Lithium-Ion Battery Pack with Air Cooling, J. Energy Eng. 145 (2019) 04019030. https://doi.org/10.1061/(asce)ey.1943-7897.0000631.

[10] X. Yang, T. Liu, S. Ge, Y. Leng, D. Wang, X. Yang, T. Liu, Y. Gao, S. Ge, Y. Leng, D. Wang, Asymmetric Temperature Modulation for Extreme Fast Charging of Lithium-Ion Batteries, Joule. 3 (2019) 3002–3019. https://doi.org/10.1016/j.joule.2019.09.021.

[11] M. Broussely, S. Herreyre, P. Biensan, P. Kasztejna, K. Nechev, R.J. Staniewicz, Aging mechanism in Li ion cells and calendar life predictions, J. Power Sources. 97–98 (2001) 13–21. https://doi.org/10.1016/S0378-7753(01)00722-4.

[12] R. Spotnitz, J. Franklin, Abuse behavior of high-power, lithium-ion cells, J. Power Sources. (2003). https://doi.org/10.1016/S0378-7753(02)00488-3.

[13] P. Liu, J. Wang, J. Hicks-Garner, E. Sherman, S. Soukiazian, M. Verbrugge, H. Tataria, J. Musser, P. Finamore, Aging Mechanisms of LiFePO[sub 4] Batteries Deduced by Electrochemical and Structural Analyses, J. Electrochem. Soc. 157 (2010) A499. https://doi.org/10.1149/1.3294790.

[14] M.B. Pinson, M.Z. Bazant, Theory of SEI Formation in Rechargeable Batteries: Capacity Fade, Accelerated Aging and Lifetime Prediction, J. Electrochem. Soc. 1601608 (2013) 243–250. https://doi.org/10.1149/2.044302jes.

[15] S. Ahmed, I. Bloom, A.N. Jansen, T. Tanim, E.J. Dufek, A. Pesaran, A. Burnham, R.B. Carlson, F. Dias, K. Hardy, M. Keyser, C. Kreuzer, A. Markel, A. Meintz, C. Michelbacher, M. Mohanpurkar, P.A. Nelson, D.C. Robertson, D. Scoffield, M. Shirk, T. Stephens, R. Vijayagopal, J. Zhang,

Enabling fast charging – A battery technology gap assessment, J. Power Sources. 367 (2017) 250–262. https://doi.org/10.1016/j.jpowsour.2017.06.055.

[16] Z. Du, D.L.W. Iii, I. Belharouak, Enabling fast charging of high energy density Li-ion cells with high lithium ion transport electrolytes, Electrochem. Commun. 103 (2019) 109–113. https://doi.org/10.1016/j.elecom.2019.04.013.

[17] I.H. Son, J.H. Park, S. Park, K. Park, S. Han, J. Shin, S. Doo, Y. Hwang, H. Chang, J.W. Choi, Graphene balls for lithium rechargeable batteries with fast charging and high volumetric energy densities, Nat. Commun. 8 (2017). https://doi.org/10.1038/s41467-017-01823-7.

[18] T. Waldmann, B.-I. Hogg, M. Kasper, S. Grolleau, C.G. Couceiro, K. Trad, B.P. Matadi, M. Wohlfahrt-Mehrens, Interplay of Operational Parameters on Lithium Deposition in Lithium-Ion Cells: Systematic Measurements with Reconstructed 3-Electrode Pouch Full Cells, J. Electrochem. Soc. 163 (2016) A1232–A1238. https://doi.org/10.1149/2.0591607jes.

[19] X. Yang, C. Wang, Understanding the trilemma of fast charging , energy density and cycle life of lithium-ion batteries, J. Power Sources. 402 (2018) 489–498. https://doi.org/10.1016/j.jpowsour.2018.09.069.

[20] M. Doyle, T.F. Fuller, J. Newman, Modeling of Galvanostatic Charge and Discharge of the Lithium/Polymer/Insertion Cell, J. Electrochem. Soc. 140 (1993) 1526–1533. https://doi.org/10.1149/2.0451908jes.

[21] J. Newman, K.E. Thomas-Alyea, Electrochemical Systems, 3rd ed., WILEY, 2004.

[22] W. Fang, O.J. Kwon, C.Y. Wang, Electrochemical-thermal modeling of automotive Li-ion batteries and experimental validation using a three-electrode cell, Int. J. Energy Res. 34 (2010) 107–115. https://doi.org/10.1002/er.1652.

[23] Y. Ji, Y. Zhang, C.-Y. Wang, Li-Ion Cell Operation at Low Temperatures, J. Electrochem. Soc. J.

Electrochem. Soc. 160 (2013) 636–649. https://doi.org/10.1149/2.047304jes.

[24] W.B. Gu, C.Y. Wang, Thermal-Electrochemical Modeling of Battery Systems, J. Electrochem. Soc. 147 (2000) 2910–2922.

[25] J. Kalupson, G. Luo, C.E. Shaffer, AutoLion^{TM}: A Thermally Coupled Simulation Tool for Automotive Li-Ion Batteries, SAE Int. 1 (2013). https://doi.org/10.4271/2013-01-1522.

[26] X.G. Yang, T. Liu, S. Ge, E. Rountree, C.Y. Wang, Challenges and key requirements of batteries for electric vertical takeoff and landing aircraft, Joule. 5 (2021) 1644–1659. https://doi.org/10.1016/j.joule.2021.05.001.

[27] P. LIMA, Samsung SDI 94 Ah battery cell full specifications, Https://Pushevs.Com/2018/04/05/Samsung-Sdi-94-Ah-Battery-Cell-Full-Specifications/. (2021).

[28] P. Arora, Mathematical Modeling of the Lithium Deposition Overcharge Reaction in Lithium-Ion Batteries Using Carbon-Based Negative Electrodes, J. Electrochem. Soc. 146 (1999) 3543. https://doi.org/10.1149/1.1392512.

[29] R. V. Bugga, M.C. Smart, Lithium Plating Behavior in Lithium-Ion Cells, in: 2010: pp. 241–252. https://doi.org/10.1149/1.3393860.

[30] Y. Ji, Y. Zhang, C.-Y. Wang, Li-Ion Cell Operation at Low Temperatures, J. Electrochem. Soc. 160 (2013) A636–A649. https://doi.org/10.1149/2.047304jes.

[31] M.D. Levi, D. Aurbach, Diffusion Coefficients of Lithium Ions during Intercalation into Graphite Derived from the Simultaneous Measurements and Modeling of Electrochemical Impedance and Potentiostatic Intermittent Titration Characteristics of Thin Graphite Electrodes, J. Phys. Chem. B. 101 (1997) 4641–4647. https://doi.org/10.1021/jp9701911.

[32] N. Takami, Structural and Kinetic Characterization of Lithium Intercalation into Carbon Anodes for Secondary Lithium Batteries, J. Electrochem. Soc. 142 (1995) 371.

https://doi.org/10.1149/1.2044017.

[33] J. Landesfeind, J. Hattendorff, A. Ehrl, W.A. Wall, H.A. Gasteiger, Tortuosity Determination of Battery Electrodes and Separators by Impedance Spectroscopy, J. Electrochem. Soc. 163 (2016) A1373–A1387. https://doi.org/10.1149/2.1141607jes.

[34] L.O. Valøen, J.N. Reimers, Transport Properties of LiPF[sub 6]-Based Li-Ion Battery Electrolytes, J. Electrochem. Soc. 152 (2005) A882. https://doi.org/10.1149/1.1872737.

[35] M.W. Verbrugge, B.J. Koch, J.E. Soc, M.W. Verbrugge, B.J. Koch, Electrochemical Analysis of Lithiated Graphite Anodes, J. Electrochem. Soc. 150 (2003). https://doi.org/10.1149/1.1553788.

[36] L. Sheng, L. Su, H. Zhang, Y. Fang, H. Xu, W. Ye, An improved calorimetric method for characterizations of the specific heat and the heat generation rate in a prismatic lithium ion battery cell, Energy Convers. Manag. 180 (2019) 724–732. https://doi.org/10.1016/j.enconman.2018.11.030.

[37] D. Kim, J. Kang, T. Eom, J. Kim, J. Lee, C. Won, An Adaptive Rapid Charging Method for Lithium-Ion Batteries with Compensating Cell Degradation Behavior, Appl. Sci. 8 (2018) 1–12. https://doi.org/10.3390/app8081251.

[38] C.Y. Wang, G. Zhang, S. Ge, T. Xu, Y. Ji, X.G. Yang, Y. Leng, Lithium-ion battery structure that self-heats at low temperatures, Nature. 529 (2016) 515–518. https://doi.org/10.1038/nature16502.

[39] X.G. Yang, T. Liu, C.Y. Wang, Innovative heating of large-size automotive Li-ion cells, J. Power Sources. 342 (2017) 598–604. https://doi.org/10.1016/j.jpowsour.2016.12.102.